

Towards Pedestrian Dead Reckoning and Incline Estimation on the Össur Power Knee

Nana Porter-Honicky

*Dept. of Mechanical Engineering
University of Michigan
Ann Arbor, USA
narmph@umich.edu*

Anushka Rathi

*Dept. of Mechanical Engineering
University of Michigan
Ann Arbor, USA
anushkar@umich.edu*

C. Andrew Seelhoff

*Dept. of Mechanical Engineering
University of Michigan
Ann Arbor, USA
seelhoff@umich.edu*

Abstract—This study explores the feasibility of using the limited sensor suite of the Össur Power Knee to estimate gait speed and incline in a pilot study. We use a Kalman filter approach for fusing accelerometer and gyroscope signals from the shank-mounted inertial measurement unit (IMU) to estimate sensor orientation and transform IMU accelerations into the global frame. Stride segmentation is performed using thresholds on Power Knee’s strain gauge signals to identify gait events. We then utilize pedestrian dead reckoning techniques to estimate shank position over time. We remove gravity from the global frame acceleration, use trapezoid integration to estimate velocity and position, and apply zero-velocity updates per stride to minimize drift. From the reconstructed motion, we derive estimates of walking speed and terrain slope. Although this work is limited to a single participant and short walking bouts, preliminary results suggest that meaningful task-level insights can be estimated even with the limited sensor suite on the Power Knee.

Index Terms—dead reckoning, powered prosthesis, Kalman filter

I. INTRODUCTION

Over two million people in the United States, and nearly 60 million people globally, are estimated to be living with limb loss, with these prevalence totals forecast to increase further in the coming decades [1]–[3]. In recent years, significant advancements have been made in powered leg prostheses, which provide positive work during the gait cycle, unlike many existing passive prostheses. While these devices have begun to show benefits over the state of the art [4], there remains a large gap in the translation of cutting-edge prosthetic technology to commercial devices.

Many research devices, including the one outlined in [5], consist of powered knee and ankle joints, allowing biomimetic ranges of motion in both joints at the expense of distal weight and computational complexity. While these setbacks can be mitigated in a laboratory setting, they are too costly for real-world use, and as such, current commercially available powered knee prostheses pair their devices with passive Energy Storage and Return (ESR) feet. These *powered-knee, passive-ankle* systems allow for powered assistance without major weight increases compared to standard-of-care prostheses, as the weight difference between powered and passive knees is substantially lower than that of powered and passive ankles.

One downside to using an ESR foot, however, is the reduced range of motion (RoM) compared to an able-bodied ankle [6]. ESR feet are designed to mimic the RoM and overall behavior of the human ankle on level ground [7] and as such can largely replicate normative kinematics on this terrain. However, ESR feet cannot replicate larger ankle range of motion observed in other activities, such as ramps or stairs, resulting in users exhibiting compensatory gait behaviors [8]–[10].

A. Össur Power Knee

While there are multiple adaptive dissipation knees (passive devices) on the market such as the C-Leg (Ottobock, Duderstadt, Germany), Rheo Knee (Össur , Reykjavik, Iceland), Adaptive2 (Blatchford, Basingstoke, UK), and Synergy knee [11], [12] there has only been one knee on the market that provides active torque until very recently, the Össur Power Knee. In powered devices, the most critical “component”, for a useful device is the control strategy. The current state of the art for control strategies of powered lower limb prostheses is Hybrid Kinematic Impedance Control (HKIC) [13]. However, people navigate across many different terrains and the controller must be able to adapt to them quickly to make it usable outside of a highly controlled setting. To do this, we need to incorporate terrain estimation into our controller.

B. Control of Powered Knee Prostheses

Recent efforts have been made to translate HKIC [13], a continuous biomimetic control paradigm originally deployed on experimental hardware [5], onto the Power Knee (Össur hf, Reykjavik, Iceland), a commercially available powered knee prosthesis. The Power Knee is paired with a low-profile ESR foot to maximize the range of users which can wear the device and as such exhibits substantially lower ankle RoM than the human ankle. As the controller in [13] implicitly assumes normative ranges of motion at its joints, adaptations to knee control must be made to account for both the lack of ankle control and the limited ankle motion provided by the ESR foot. Level-walking and Sit/Stand behaviors required minimal alterations to the existing framework [14], and preliminary work has been done to adapt the controller for navigation of inclines [15]. For a given speed and incline, there exists an optimal trajectory which the Power Knee attempts to push the

knee joint towards. However, the existing controllers in [15] must be manually selected using ground-truth knowledge of the *gait task*, preventing real-world adaptation across inclines.

Incline and speed classification is often modeled as a mid-level control problem, where these indicators of task are fed into a control model to refine target inputs and trajectories. Research devices typically have access to a wide range of sensors and data formats which can be used to intuit the environment in which the leg is navigating: for example, Leg2 from the University of Michigan [5] has inertial measurement units located on both the foot and the hip, providing reliable estimates of orientation and more crucially, the angle of the foot at all times. The difficulty with translating the HKIC control paradigm to Össur Power Knee from Leg2 is the comparatively limited on-board sensor suite: There is only one IMU at the shank, four strain gauge sensors placed near the bottom corners of the knee, and an encoder at the knee joint.

C. Pedestrian Dead Reckoning

Pedestrian dead reckoning [16], a method of estimating sensor position based on previous measurements, has been used for online estimates of walking path and gait parameters (i.e. joint positions) [17]. It has also been used for heuristic terrain estimation on a powered ankle prosthesis [18]. Stride segmentation for pedestrian dead reckoning is typically done by utilizing a zero velocity update method (ZUPT) for stride segmentation where it assumed that the knee has zero velocity when the shank is perpendicular to ground [19]. This addresses much of the drift associated with the integration of accelerometer signals. Using method a similar to that of [18] with the IMU sensor on board the Össur Power Knee would allow for an easy transition between different task specific controllers that have already been deployed and tested on the device [14], [15].

II. METHODS

A. Data Collection

This pilot study comprised one above-knee amputee participant (male, age 24). The participant used the Power Knee and a correctly-sized Pro-Flex LP ESR foot (Össur hf, Reykjavik, Iceland). The *task space* spanned forward walking speeds of 0.8, 1.0, and 1.2 meters per second and ground slopes between -10° and $+10^\circ$ at increments of 5° . Fifteen discrete gait tasks were selected for evaluation, matching the task space used in [20]. For each gait task, the Power Knee was configured for walking at the current task, using the trajectories described in [15]. Before accelerating the treadmill to steady-state speed, the user stomped on the treadmill belt with their prosthesis. This calibration motion method was selected to synchronize the force readings of the Power Knee's strain gauges and the treadmill's force plates in post-processing. Then, the participant walked for thirty seconds at steady-state with several seconds before and after the steady-state period to allow for acceleration and deceleration.

The subject was fit with a breathable velcro suit (OptiTrack, Corvallis, OR) for ease of motion capture marker placement.

A custom motion capture marker set, shown in Figure 1, was used to identify the subject's body segments. Specific marker placements on the body, along with their naming conventions, are denoted in Table I. A motion capture system (VICON, Oxford, UK) was used to record 3D positions and sampled at 250 Hz. An instrumented treadmill (Bertec Corporation, Columbus, OH) collected ground reaction force (GRF) data at 1 kHz.



Fig. 1: Marker placements as seen on the lateral side of the body using the modified Rajagopal set.

Body Segment	Markers Used				
Torso	C7	STRN	L/R SHO		
Femur	L/R THI1	L/R THI2	L/R THI3	L/R LKN	L/R MLKN
Tibia	L/R TIB1	L/R TIB2	L/R TIB3	L/R LANK	L/R MANK
Foot	L/R MET1	L/R MET2	L/R MET5	L/R HEE	
Pelvis	L/R ASIS	L/R PSIS			

TABLE I: Marker set used to identify body segments. L (left), R (right)

Embedded within the Össur Power Knee is a six-axis shank-mounted IMU inclusive of an accelerometer and gyroscope. Additionally, there are streams of four strain gauges and a knee encoder available to record. Power Knee data was collected with a sampling frequency of 50 Hz.

Data collected in this experiment include GRF from the instrumented treadmill, motion capture marker trajectories, IMU signals, and strain gauge signals from the Power Knee. Motion capture data was processed in OpenSim 4.5 (Stanford, CA, USA) using the model from [21] with modifications made to account for the Power Knee's inertial properties, similar to [22].

B. Data Analysis

GRFs were low-pass filtered using a bidirectional fourth-order Butterworth filter with a 10 Hz cutoff frequency in Vicon Nexus. All marker data was rigid-body gap-filled and low-pass filtered using a bidirectional fourth-order Butterworth filter with a 6 Hz cut-off frequency in Vicon Nexus. Marker data was then processed using a custom OpenSim pipeline to calculate joint kinematics and kinetics. These are used as validation for the position data found through IMU estimations. MATLAB R2024b (MathWorks, Natick, MA) was used

for all post-processing of Power Knee and VICON data. The IMU accelerations, angular velocities, and strain gauges were low-pass filtered using a bidirectional fourth-order Butterworth filter with a 10 Hz cutoff frequency.

C. Kalman Filter

To obtain orientation estimates from our filtered acceleration and angular velocity data, we utilize the built-in MATLAB function *imufilter*. This function applies a Kalman filter to fuse accelerometer and gyroscope data using the sampling frequency, providing a stable estimate of orientation and angular velocity over time. Filter parameters were chosen based on the Power Knee's IMU and its corresponding datasheet. At each time step, *imufilter* will estimate the sensor orientation from the acceleration and gyroscope readings and output a quaternion. We then rotate the acceleration vector by the current orientation quaternion to obtain our accelerations and angular velocities in the global frame. Figure 2 displays the Power Knee's local frame and the laboratory, or global frame. We converted our orientation quaternion to ZXY Euler angles to facilitate matrix multiplication of our acceleration and gyroscope measurement vectors. Because the Power Knee is ideally aligned with the X-Y origin, our Z-direction angle should be the smallest. The X-direction rotations are slightly larger, but the Y-direction rotation, corresponding with the Power Knee axis of rotation, is the largest and thus saved as the final rotation.

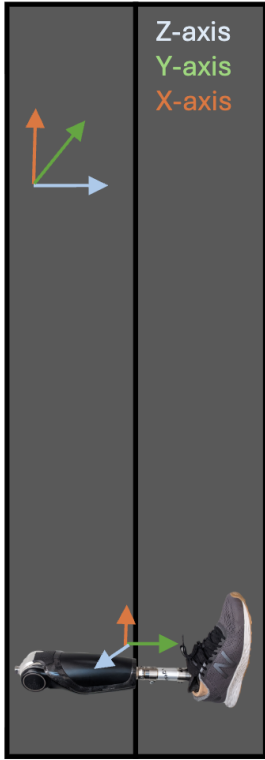


Fig. 2: Local frame of the shank IMU compared to global frame depicted on the laboratory's treadmill.

D. Dead Reckoning

To segment data into strides, we identify heel-strike and toe-off by thresholding the cumulative output of the Power Knee's four strain gauges, with units in mN . Heel strikes occur at the first reading above 125 and toe-offs occurring at the first reading below 75. The first and last strides were discarded to exclude strides occurring during the treadmill's acceleration and deceleration and only capture steady-state motion.

Within each stride, while the prosthetic foot has contact with the ground, we identified our respective zero update (ZUPT) of the j th stride as the point in which the 2-norm of angular velocity, as calculated by the Kalman filter, is at its local minimum:

$$ZUPT(j) = \arg \min_{t \in [t_{HS}, t_{TO}]} \|\omega(t)\|_2 \quad (1)$$

where t_{HS} and t_{TO} represent the heel-strike and toe-off times of the j th stride.

Dead reckoning calculations for each stride start at $ZUPT(j)$ and end at $ZUPT(j+1)$, except for the last stride, which uses the time of the final heel strike (the one which is excluded from processing.)

The global frame accelerations calculated from the Kalman Filter are parsed into the identified strides with gravity removed. Velocity is calculated using numerical trapezoidal integration in MATLAB and corrected with our zero-velocity updates, assuming the end of a stride will result in zero shank velocity. Position is calculated through a second trapezoidal integration of the corrected velocity.

Because motion is confined to a treadmill where mediolateral motion is negligible, we can assume all motion in the X-Y plane should approximately correspond to purely "forward" (i.e. positive-X direction in the global frame) motion. As such, the estimated path distance traveled per stride is calculated as the 2-norm of the X-Y position vector found from dead reckoning. Vertical distance traveled per stride is calculated as the Z-component of the integrated position.

E. Incline and Speed Estimation

With individual stride motions calculated, we then estimated the gait task which corresponds with the observed motions in order to compare them with ground-truth data. We define the gait task $\chi = (\nu, \gamma)$ with a walking speed ν and ground slope γ , with their respective estimates $\hat{\nu}$ and $\hat{\gamma}$.

Walking speed for the j th stride is calculated as the path distance divided by stride time:

$$\hat{\nu}(j) = PATH(j)/dt(j) \quad (2)$$

Ground slope is estimated by calculating the arctangent of the path and vertical distances traveled:

$$\hat{\gamma}(j) = \arctan(\Delta z / PATH(j)) \quad (3)$$

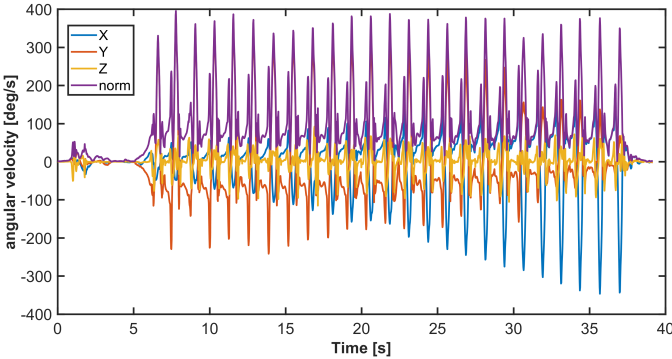
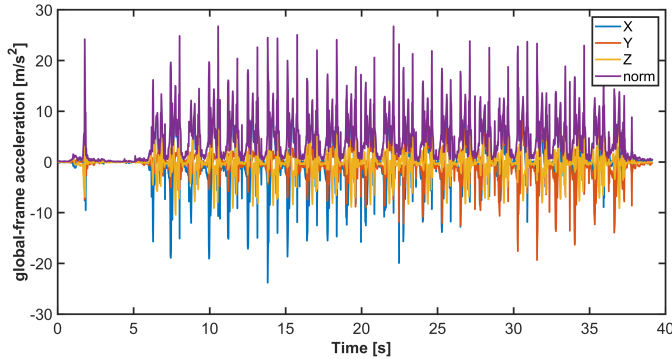


Fig. 3: Global frame accelerations and angular velocities for trial on level ground at 1 meter per second.

III. RESULTS

A. Kalman Filter

Using the orientation estimates from MATLAB's *imufilter*, we computed global-frame accelerations from the IMU data. The filter fuses accelerometer and gyroscope measurements to estimate the sensor's orientation over time and allows us to find the rotation matrix to rotate acceleration signals into the global coordinate frame. Figure 3 shows the global-frame accelerations and angular velocities as calculated from the Kalman Filter from the level-ground, 1 meter per second trial, and Figure 4 shows the orientation estimate over time from the same trial.

The lack of magnetometer data explains the drift in orientation. While heading stays constant for the first portion of the trial, the X-axis rotation begins to drift over time. While this has implications for long-term dead reckoning of the entire trial, it has a relatively small effect on the individual movements of each stride, as we know the true motion is constrained in the Y-axis and Z-axis directions.

B. Dead Reckoning

Using dead reckoning, we estimated the relative shank motion across multiple strides for each gait task given global-frame accelerations. Stride segmentation using the Power Knee's strain gauges and gyroscope allowed for consistent stride identification. Table II provides distributions of stride

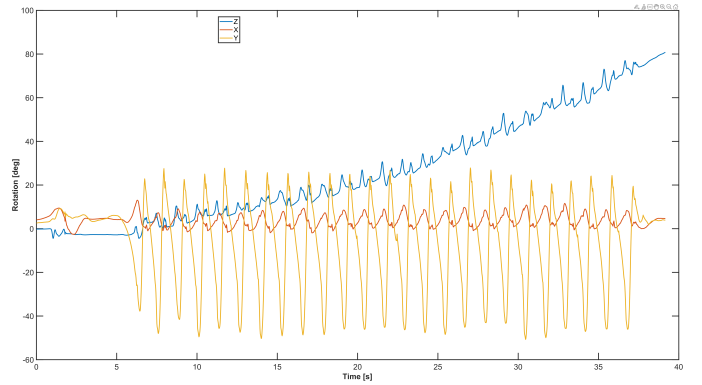


Fig. 4: ZXY Euler Angle sequence, note the drift over time in the Z axis(blue)

	0.8 m/s			1.0 m/s			1.2 m/s		
	n	\bar{x}	σ	n	\bar{x}	σ	n	\bar{x}	σ
-10°	21	1.45	0.06	24	1.28	0.03	28	1.17	0.04
-5°	23	1.30	0.04	23	1.20	0.04	27	1.06	0.03
0°	18	1.43	0.04	22	1.24	0.04	24	1.14	0.02
+5°	18	1.54	0.07	22	1.33	0.03	24	1.19	0.03
+10°	21	1.52	0.08	23	1.35	0.04	26	1.17	0.03

TABLE II: Stride Durations across tasks. n, \bar{x} , and σ denote the number of strides, average value, and standard deviation, respectively. All values are presented in seconds.

duration for each gait task, showing low variability for all tasks.

XYZ velocity estimates obtained via numerical integration using (*cumtrapz*) exhibited expected trends within each stride. Applying the zero-velocity update at the point of minimal stance phase rotational velocity reduced the error in integration for succeeding strides and aligned the shank motion to that expected in late stance phase. Figure 5 shows velocity traces for the representative trial of level ground, 1 m/s walking, denoted as *s1_i0*.

Integration of velocity using (*cumtrapz*) led to position estimates. The position estimates demonstrated general trends consistent with forward progression and vertical displacement during walking on various inclines. As expected, however, we see a significant positional drift in the Y-direction due to our drift in orientation.

When taking the X-Y magnitude for "horizontal" distance traveled, we see values which more closely match our expected stride-to-stride movement. Figure 6 provides visualization of stride trajectories from the shank across all gait tasks. Summary Statistics of Path (X-Y) and Vertical (Z) direction travel are provided in Table III.

While the overall trajectory shapes align with the expected lower-limb trajectory of the shank and foot, the position trajectory involves more downward motion than expected at all tasks. The forward distances traveled generally increase with speed, and despite the offset in vertical travel, the distances generally correlate with ground-truth incline. We calculated a correlation coefficient between ground-truth speed and estimated speed of 0.8589 and a correlation coefficient

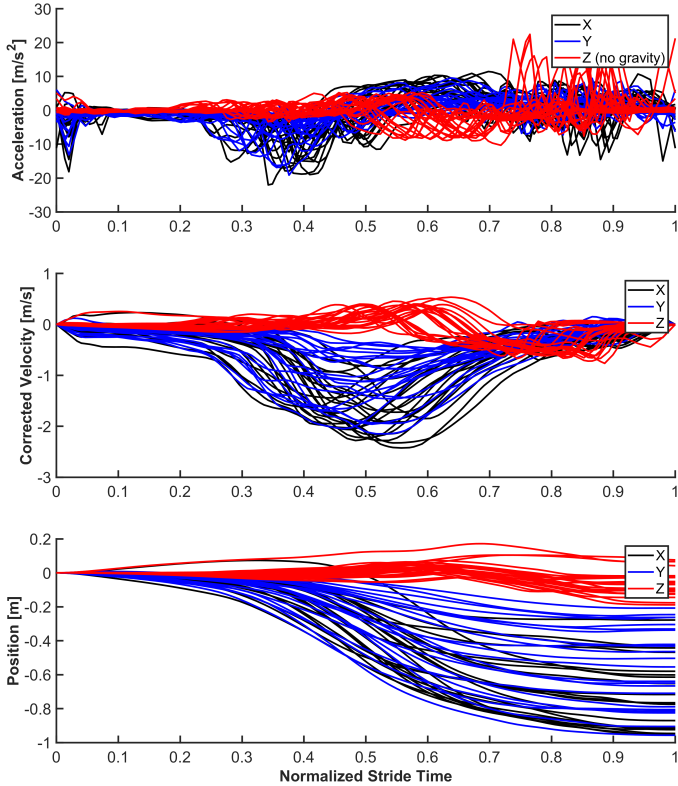


Fig. 5: Representative level-ground walking trial at 1.0 m/s. (a) Global-frame accelerations segmented by stride, with gravity removed. (b) Velocity obtained by integrating acceleration and applying zero-velocity updates at stride boundaries. (c) Shank position estimated by integrating the corrected velocity signal over each stride.

		0.8 m/s		1.0 m/s		1.2 m/s	
		\bar{x}	σ	\bar{x}	σ	\bar{x}	σ
-10°	$\hat{\nu}$ [m/s]	0.76	0.10	0.91	0.07	1.07	0.09
	$\hat{\gamma}$ [deg]	-11.39	3.15	-11.03	2.79	-11.32	2.80
-5°	$\hat{\nu}$ [m/s]	0.77	0.09	0.91	0.13	1.07	0.14
	$\hat{\gamma}$ [deg]	-5.91	2.94	-6.24	5.16	-7.29	3.91
0°	$\hat{\nu}$ [m/s]	0.69	0.08	0.76	0.11	0.90	0.12
	$\hat{\gamma}$ [deg]	-3.19	5.18	-4.06	4.49	-5.32	4.23
$+5^\circ$	$\hat{\nu}$ [m/s]	0.71	0.09	0.89	0.10	0.96	0.11
	$\hat{\gamma}$ [deg]	2.84	2.87	2.12	2.63	-1.20	3.27
$+10^\circ$	$\hat{\nu}$ [m/s]	0.78	0.10	0.92	0.11	0.96	0.20
	$\hat{\gamma}$ [deg]	8.42	1.60	7.58	3.57	6.48	4.53

TABLE IV: Task Estimates across all trials. The outermost inclines and speeds represent the ground truth task $\chi = (\nu, \gamma)$. Sample means and standard deviations are provided at each ground-truth task for the task estimate $\hat{\chi} = (\hat{\nu}, \hat{\gamma})$.

between ground-truth incline and estimated incline of 0.6283.

C. Incline and Speed Estimation

The accumulated errors in distance traveled inform errors in task estimation compared to ground truth. Figure 7 and Table IV provide distributions of task estimates across all trials. The increased negative-Z-direction travel results in incline estimates trending towards more negative slopes than expected across all activities.

IV. DISCUSSION

A key observation is the high variability present in the constructed position profiles across tasks. One contributing factor may be that individuals with amputation generally have more variable gait compared to able-bodied gait [23]. Variability could also be affected as we utilized a novel position-based controller that is still undergoing refinement [15]. Unlike impedance-based prosthetic controllers, which allow for smoother and more adaptive gait [13], position controllers can produce more abrupt deviations when user behavior departs from the expected trajectory.

Interestingly, the position traces of the shank in Figure 6 all trend further downward than the ground-truth trajectory of the current slope. One hypothesis for this result is the prosthetic foot's ability to deflect vertically under loading. Unlike biological ankles, the carbon fiber spring will visibly deflect under loading and as such, downward vertical motion continues beyond heel strike and into early stance phase. It is likely, especially given our relatively low sample rate of 50 Hz, that residual downward acceleration was recorded past initial ground contact, resulting in the shank position trace "sinking." Table IV also shows for all ground-truth inclines except -10° , there may be trends where estimated slope becomes more negative at higher speed. Higher walking speed results in faster impacts during heel strike, which could explain this behavior, although high variance in incline estimates across all ground-truth tasks makes it difficult to come to a definitive conclusion.

We additionally observe significant drift in estimated heading of the IMU, calculated as the Z-direction rotation from our ZXY Euler Angle sequence shown in Figure 4. The

		0.8 m/s		1.0 m/s		1.2 m/s	
		\bar{x}	σ	\bar{x}	σ	\bar{x}	σ
-10°	ΔXY	1.12	0.15	1.19	0.13	1.29	0.14
	ΔZ	-0.23	0.07	-0.23	0.06	-0.26	0.07
-5°	ΔXY	1.01	0.15	1.12	0.20	1.16	0.18
	ΔZ	-0.11	0.05	-0.13	0.10	-0.15	0.08
0°	ΔXY	1.01	0.12	0.96	0.11	1.05	0.10
	ΔZ	-0.06	0.09	-0.07	0.07	-0.10	0.08
$+5^\circ$	ΔXY	1.12	0.16	1.22	0.15	1.17	0.14
	ΔZ	0.06	0.06	0.05	0.05	-0.03	0.06
$+10^\circ$	ΔXY	1.22	0.18	1.27	0.17	1.15	0.24
	ΔZ	0.18	0.04	0.17	0.07	0.12	0.06

TABLE III: Distances traveled per stride, between zero-velocity update points, across all tasks. All values are provided in meters. ΔXY denotes path-distance traveled along the X-Y axes, calculated as the 2-norm. ΔZ corresponds to vertical displacement of the shank.

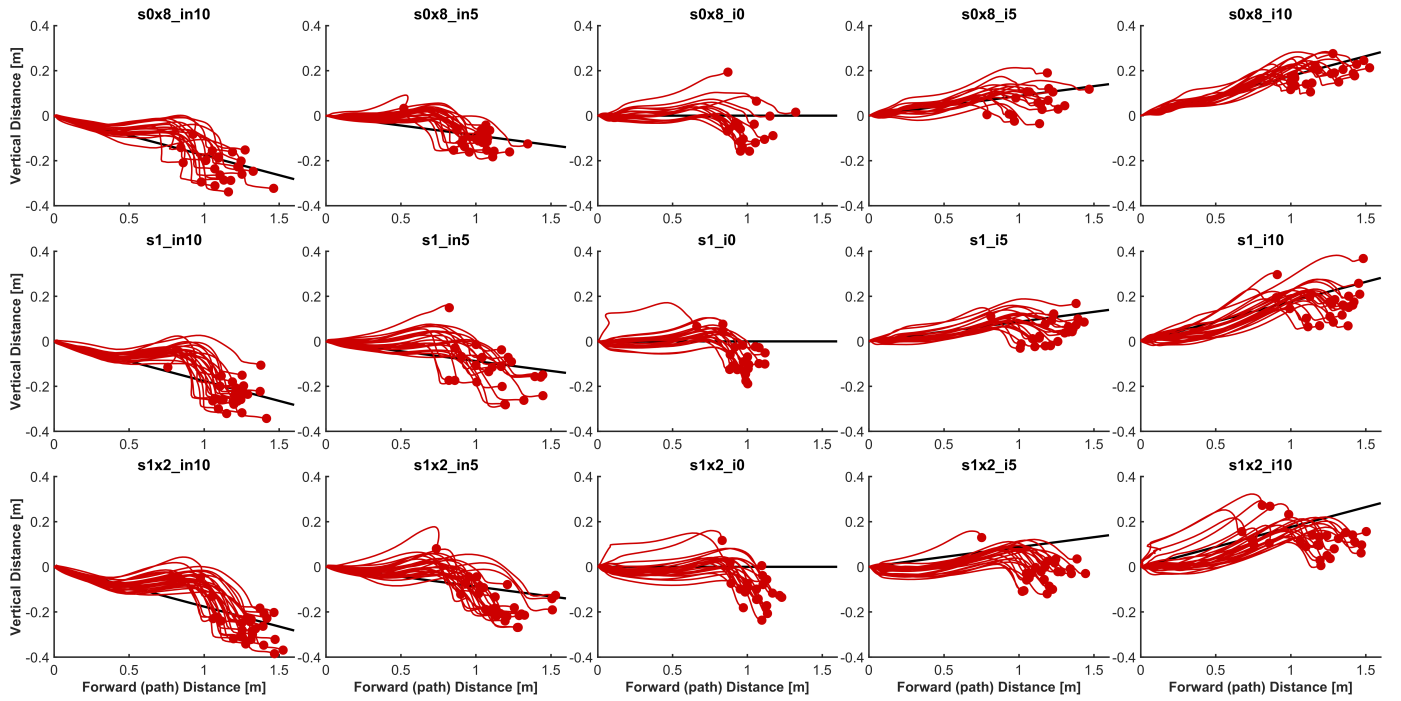


Fig. 6: Dead Reckoning Position Traces across all tasks. Black lines indicate the ground-truth slope of the treadmill for the trial. Inclines are read as i , followed by n if negative, followed by the incline in degrees. Speeds are read as s , followed by (ones digit) x (tenths place). For example, $s0x8_i0$ corresponds to 0.8 m/s speed, 0 degrees slope.

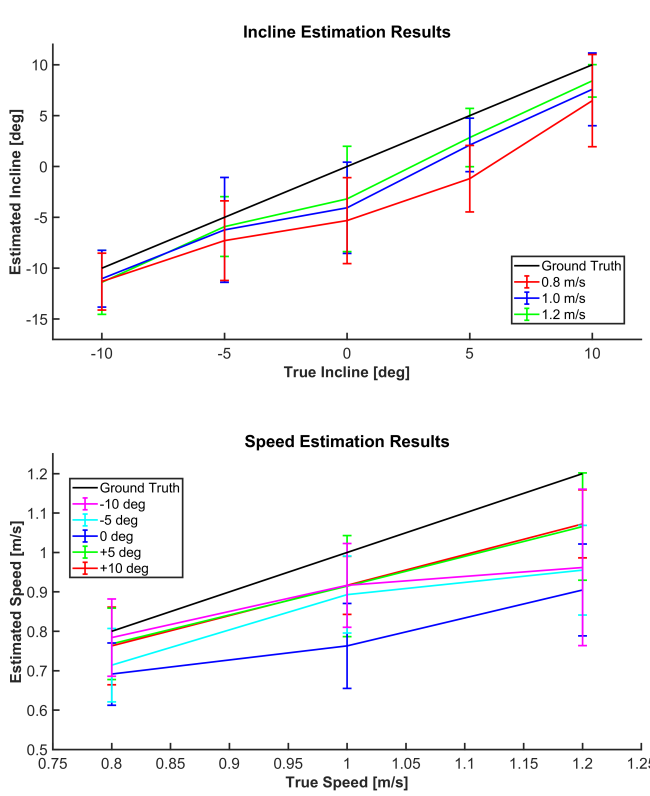


Fig. 7: Task Estimates across all trials, compared to ground-truth values.

X- and Y-direction rotations of this Euler Angle series are relatively stable, which suggests our primary axes of motion are being calculated and registered correctly. Ideally, with a magnetometer or other method to correct for drift, we would have been able to directly use the change in X-direction distance as our "path" distance rather than the 2-norm of X-Y distance traveled. Because the treadmill motion is largely confined to the X-direction, we can assume true global frame Y-direction travel is negligible. Although this assumption does not affect stride-by-stride dead reckoning, it does compromise the current algorithm's capability to estimate total distance traveled, as the drifting heading will cause the walking data to appear to continually turn left over time.

Excessive downward movement seems to occur across all gait tasks. One potential explanation for this repeated behavior is more acceleration recorded by the shank than what actually occurs during early stance phase. As the heel is loaded after heel strike, the foot begins to compress until fully loaded. This vertical movement after contact is near-zero, but the decreased rate of deceleration results in more vertical movement being recorded through dead reckoning.

Despite these challenges, we observe low deviations in stride duration and consistent trends in XY position. This suggests that with improved calibration and processing, dead reckoning from this minimal sensor set could feasibly support more accurate and less variable estimates of incline and speed.

A. Limitations and Future Work

This analysis is based on pilot data from a single participant ($n = 1$), using an experimental control paradigm. This cannot allow for any assessment of statistical significance or generalizability of this method. Additionally, it should be noted that each task was recorded with only one trial and included only 20-30 strides. This limits both the amount of the data available and the robustness of determining speed and incline estimations. Longer trials with a higher IMU sampling rate, in addition to use of a more refined controller, would greatly improve the quality of the collected data and thus our dead reckoning trajectories and resulting task estimates.

Another key limitation was the absence of the magnetometer signals from the IMU. Without the heading correction, the orientation estimates relied solely on gyroscope and accelerometer inputs. This increases the susceptibility of sensor drift with time. This could have contributed to the errors observed in the dead reckoning position estimates with respect to the large drifts in the mediolateral position estimation.

Finally, while post-hoc estimation has proven useful for assessing feasibility, real-time implementation is essential for practical use in prosthetics. Future efforts should focus on creating algorithms for real-time processing onboard the Össur Power Knee to allow for the estimation of terrain slope and walking speed in real-world settings.

To evaluate the effects of the proposed changes above, future work will compare the implemented dead reckoning approach against ground-truth kinematics obtained from motion capture systems. This comparison can help quantify the accuracy of position and velocity estimates.

V. CONCLUSION

This pilot study highlights several key challenges in implementing dead reckoning with limited sensor data. The absence of magnetometer input contributed to orientation drift over time, which propagated errors into velocity and position estimates. These downstream effects highlight the importance of reliable orientation correction if using IMU data in estimating position or other metrics using position.

Accurate stride segmentation is key when applying a zero-velocity correction. This correction is a critical step in reducing drift with numerical integration. Inconsistent or inaccurate segmentation can reduce the robustness of dead reckoning.

Though difficult, these preliminary results suggest that it may still be possible to use a limited IMU sensor suite to estimate the terrain slope and walking speed when using a powered prosthesis.

REFERENCES

- [1] K. Ziegler-Graham, E. J. MacKenzie, P. L. Ephraim, T. G. Travison, and R. Brookmeyer, "Estimating the Prevalence of Limb Loss in the United States: 2005 to 2050," *Archives of Physical Medicine and Rehabilitation*, vol. 89, pp. 422–429, Mar. 2008.
- [2] C. L. McDonald, S. Westcott-McCoy, M. R. Weaver, J. Haagsma, and D. Kartin, "Global prevalence of traumatic non-fatal limb amputation," *Prosthetics & Orthotics International*, vol. 45, pp. 105–114, Apr. 2021.
- [3] M. Caruso and S. Harrington, "Prevalence of Limb Loss and Limb Difference in the United States: Implications for Public Policy," 2024.
- [4] F. Rasheed, S. Martin, and K. M. Tse, "Design, Kinematics and Gait Analysis, of Prosthetic Knee Joints: A Systematic Review," *Bioengineering*, vol. 10, p. 773, June 2023.
- [5] T. Elery, S. Rezazadeh, C. Nesler, and R. D. Gregg, "Design and Validation of a Powered Knee–Ankle Prosthesis With High-Torque, Low-Impedance Actuators," *IEEE Trans. Robotics*, vol. 36, pp. 1649–1668, Dec. 2020.
- [6] C. L. Brockett and G. J. Chapman, "Biomechanics of the ankle," *Orthop Trauma*, vol. 30, p. 232, June 2016.
- [7] A. H. Hansen, D. S. Childress, S. C. Miff, S. A. Gard, and K. P. Mesplay, "The human ankle during walking: implications for design of biomimetic ankle prostheses," *Journal of Biomechanics*, vol. 37, pp. 1467–1474, Oct. 2004.
- [8] A. H. Vrielink, H. G. van Keeken, T. Schoppen, E. Otten, J. P. K. Halbertsma, A. L. Hof, and K. Postema, "Uphill and downhill walking in unilateral lower limb amputees," *Gait & Posture*, vol. 28, pp. 235–242, Aug. 2008.
- [9] D. C. Morgenroth, M. Roland, A. L. Pruziner, and J. M. Czerniecki, "Transfemoral amputee intact limb loading and compensatory gait mechanics during down slope ambulation and the effect of prosthetic knee mechanisms," *Clin. Biomechanics*, vol. 55, pp. 65–72, June 2018. Publisher: Elsevier.
- [10] T. Schmalz, S. Blumentritt, and B. Marx, "Biomechanical analysis of stair ambulation in lower limb amputees," *Gait & Posture*, vol. 25, pp. 267–278, Feb. 2007.
- [11] E. Martinez-Villalpando, L. Mooney, G. Elliott, and H. Herr, "Antagonistic active knee prosthesis. A metabolic cost of walking comparison with a variable-damping prosthetic knee," *Conference proceedings : ... Annual International Conference of the IEEE Engineering in Medicine and Biology Society. IEEE Engineering in Medicine and Biology Society. Conference*, vol. 2011, pp. 8519–22, Aug. 2011.
- [12] M. Bellmann, T. Schmalz, E. Ludwigs, and S. Blumentritt, "Immediate Effects of a New Microprocessor-Controlled Prosthetic Knee Joint: A Comparative Biomechanical Evaluation," *Archives of Physical Medicine and Rehabilitation*, vol. 93, pp. 541–549, Mar. 2012.
- [13] T. K. Best, C. G. Welker, E. J. Rouse, and R. D. Gregg, "Data-Driven Variable Impedance Control of a Powered Knee–Ankle Prosthesis for Adaptive Speed and Incline Walking," *IEEE Transactions on Robotics*, vol. 39, pp. 2151–2169, June 2023.
- [14] T. K. Best, C. A. Seelhoff, and R. D. Gregg, "Implementation and Validation of a Data-Driven Variable Impedance Controller on the Össur Power Knee," in *Int. Conf. Rehabilitation Robotics 2025*, 2025.
- [15] C. A. Seelhoff, T. K. Best, and R. D. Gregg, "Adapting Biomimetic Kinematics for Controlling a Powered-Knee, Passive-Ankle Prosthesis Across Inclines," in *Int. Conf. Rehabilitation Robotics 2025*, 2025.
- [16] S. Beauregard and H. Haas, "Pedestrian dead reckoning: A basis for personal positioning," *Proceedings of the 3rd Workshop on Positioning, Navigation and Communication (WPNC'06)*, Jan. 2006.
- [17] T. Bennett, R. Jafari, and N. Gans, "An Extended Kalman Filter to Estimate Human Gait Parameters and Walking Distance," *Proceedings of the ... American Control Conference. American Control Conference*, vol. 2013, pp. 752–757, June 2013.
- [18] R. Stolyarov, M. Carney, and H. Herr, "Accurate Heuristic Terrain Prediction in Powered Lower-Limb Prostheses Using Onboard Sensors," *IEEE Transactions on Biomedical Engineering*, vol. 68, pp. 384–392, Feb. 2021.
- [19] L. Ojeda and J. Borenstein, "Non-GPS Navigation for Security Personnel and First Responders," *Journal of Navigation*, vol. 60, pp. 391–407, Sept. 2007.
- [20] E. Reznick, K. R. Embry, R. Neuman, E. Bolívar-Nieto, N. P. Fey, and R. D. Gregg, "Lower-limb kinematics and kinetics during continuously varying human locomotion," *Scientific Data*, vol. 8, p. 282, Oct. 2021. Number: 1 Publisher: Nature Publishing Group.
- [21] A. Rajagopal, C. L. Dembia, M. S. DeMers, D. D. Delp, J. L. Hicks, and S. L. Delp, "Full-Body Musculoskeletal Model for Muscle-Driven Simulation of Human Gait," *IEEE Transactions on Biomedical Engineering*, vol. 63, pp. 2068–2079, Oct. 2016.
- [22] V. Raveendranathan, V. G. M. Kooiman, and R. Carloni, "Musculoskeletal model of osseointegrated transfemoral amputees in OpenSim," *PLOS ONE*, vol. 18, p. e0288864, Sept. 2023. Publisher: Public Library of Science.
- [23] H. Keklicek, E. Kirdi, A. Yalcin, S. Topuz, O. Ulger, F. Erbahceci, and G. Sener, "Comparison of gait variability and symmetry in trained individuals with transtibial and transfemoral limb loss," *Journal of Or-*

thopaedic Surgery, vol. 27, p. 2309499019832665, Jan. 2019. Publisher:
SAGE Publications Ltd STM.